Tikrit Journal of Engineering Sciences

IRAQI Academic Scientific Journals | TJES Tikrit Journal of Engineering Sciences

Article | Tikrit Journal of Engineering Sciences (2026); 33(3): 2645

Open Access

A Miniaturized 5.8 GHz L-Shaped Antenna Structure Modelled with Doubler-Multiplier Circuit Topologies

Saad G. Muttlak [1*], Omar S. Abdulwahid [2], Mohammadreza Sadeghi [3], Mohamed Missous[4]

[1] Electrical Department, College of Engineering, Tikrit University, Tikrit, Iraq.
[2] Department of Mechatronics Engineering, College of Engineering, University of Mosul, Mosul, Iraq.
[3] Advanced Hall Sensors Ltd., Manchester, UK.
[4] Department of Electrical and Electronic Engineering, University of Manchester, Manchester, UK.

Emails:
Saad G. Muttlak ✉ | Omar S. Abdulwahid ✉ | Mohammadreza Sadeghi ✉ | Mohamed Missous ✉

Abstract:

This work reports the design and performance of two 5.8 GHz rectenna circuits for energy harvesting in implanted medical devices. The miniaturization technique used in the present work yields a compact L-shaped antenna of only 5 mm^2, making it highly compatible with non-surgical implantation inside the human body. The fabrication and simulation data of the antenna are well-matched, with strong performance compared with the reported structure at a similar frequency band. A -20 dB measured reflection, and -14.6 dB simulated peak gain at 5.5 GHz were obtained. The modeling results indicate that the proposed rectenna based on the Cockcroft-Walton voltage doubler produced an output voltage of 0.83 V, corresponding to an RF-to-DC conversion efficiency of 0.14% at 0 dBm RF power. Before modelling procedure, all the passive elements utilized in the rectenna configuration were fabricated and tested. A variation in the load resistor revealed that a rectenna with an integrated Dickson voltage multiplier delivered an optimum output voltage and power of 1.25 V and 5.5 µW at a 0.25 MΩ load, respectively. The Dickson voltage multiplier achieved a 0.55% conversion efficiency, matching the reported figure of merit in the literature. At a higher efficiency of 0.8% with a relatively low load, the results demonstrate the proposed topology's potential as a good candidate for a miniaturized integrated rectenna geometry utilized in high-frequency energy harvesting systems.

Keywords:

Energy harvesting technology; Compact antenna; Rectenna modelling; Implanted devices; Double-multiplier circuits.

Highlights:

- A compact L-Shaped dipole antenna for implantable medical application.
- 5mm^2 monolithically integrated rectenna operating at 5.8GHz.
- A validated circuit model is presented up to 40GHz.
- As high as 1.67V output voltage obtained from the rectenna-multiplier configuration.

Corresponding Author*:

Saad G. Muttlak ✉
Electrical Department, College of Engineering, Tikrit University, Tikrit, Iraq.

Article History:

Received:	10	Jul.	2025
Received in revised form:	25	Sep.	2025
Accepted:	30	Oct.	2025
Final Proofreading:	01	Sep.	2026
Available online:	15	Oct.	2026

Citation:

Muttlak SG, Abdulwahid OS, Sadeghi M, Missous M. **A Miniaturized 5.8 GHz L-Shaped Antenna Structure Modelled with Doubler-Multiplier Circuit Topologies**. *Tikrit Journal of Engineering Sciences* 2026; **33**(3): 2645.

https://doi.org/10.25130/tjes.33.3.1

© This Is an Open Access Article Under the cc by License. http://creativecommons.org/licenses/by/4.0/

1.INTRODUCTION

The development of modern communication systems with many electronic devices and sensors is constrained by the cost and size of battery power sources. Radio frequency (RF) energy harvesting systems offer an effective solution by collecting ambient electromagnetic waves and converting them into usable DC voltage [1]. Over the last decade, interest has grown in designing high-frequency harvesting systems because they can support wireless communication systems that require high data rates for a range of applications [2]. Integrated rectifier-antenna structures are central to such systems. Researchers have used various techniques to maximize performance while reducing the size of discrete devices. In the literature, various antenna structures have been presented for implantable devices, with the main goal of improving key performance metrics, including antenna gain, radiation efficiency, frequency bandwidth, and a reduced reflection coefficient (S_{11}). Other crucial characteristics include biomedical compatibility, miniaturization, patient safety, and tolerance to human body movements. Reducing the antenna size and volume is key to fitting comfortably inside the patient's body; however, this can degrade the antenna's efficiency and gain [2]. Different techniques have been proposed by researchers to enhance the antenna's gain, where various structures were integrated with the antenna, as well as employing lenses and parasitic components [3, 4]. Nevertheless, these proposed solutions introduced large antenna sizes, which also restricted their use inside the body. Another challenge is the biological impact of tissue, which severely affects impedance matching and alters the antenna's reflection coefficient and radiation pattern [5] because human tissue dispersion and changes in dielectric properties alter the antenna's overall dielectric response. One proposed solution is to use a high-dielectric-constant substrate with bottom and top substrate layers, however, producing a narrow frequency bandwidth and low radiation efficiency [6, 7]. The work reported in [8] presents a wide-slot antenna structure operating at 5.8 GHz for energy-harvesting systems in drones and mobile terminals. The antenna was placed on a 0.8 mm dielectric substrate with a permittivity of 2.65 and measured 41 mm × 40 mm. A rectifier circuit based on a single HSMS-286C diode and a matching circuit was used to convert the RF signal into DC voltage. At a high input power of 18 dBm, the rectenna produced an output DC voltage and conversion efficiency of 6.2 V and 65 %, respectively, when connected to a 910 Ω load. Deng et al. proposed a dual-band rectenna circuit operating at 2.4 and 5.8 GHz bands [1]. The antenna was located on a RO4350B dielectric substrate and measured 14×16 mm². Two zero-bias HSMS-2862 Schottky barrier diodes were integrated into the rectifier circuit, with a matching network implemented using shorted-stub transmission lines to maximize power transfer from the antenna to the diode. The total rectenna size, including a radial stub for harmonic suppression at the output, was 88 × 31 mm², and it produced 2.82 V DC with 60% conversion efficiency at 5.8 GHz when connected to a 1.8 kΩ load resistor. Basir and Yoo studied a high-conversion-efficiency rectenna circuit for deep-implanted medical devices [9]. The rectenna operated at a resonant frequency of 1470 MHz, based on a meandered-line patch on a Rogers RO3010 substrate as the antenna. The antenna was covered on top with a Rogers 3010 superstrate layer, occupied a small volume of 8.43 mm³, and had a peak gain of -28 dBi. A lumped-element matching network and two SMS7630 Schottky diodes served as a voltage doubler, converting the received RF signal into DC voltage. The rectenna produced an output voltage of 4V at 2 dBm input RF power. At the same power, the rectenna had a high conversion efficiency of 90% when it was implanted at a depth of 50 mm inside the human body. However, studies reported in the literature still suffer from several issues: large antenna geometry (> 180 mm²), very low antenna gain (-28 Bi), and difficulties with full rectenna integration. The present work demonstrates a 1×5 mm² rectenna doubler operating at 2.4 GHz [10]. The rectifier was integrated with a planar folded antenna, making it a strong candidate for a miniaturized integrated circuit for wireless power transfer and/or implanted biomedical applications. A planar folded structure offers several benefits, including compact size, relaxed microfabrication, making it a strong candidate, and compatibility with monolithic-integration semiconductor rectifiers. It is performed without the need for a bonding process from the antenna to the rectifier pads utilized in the hybrid integration scheme. Once the entire rectenna is enclosed in a capsule, it can be implanted under the patient's tissue using conventional medical syringes with typical inner needle diameters of 1.6–1.1 mm [11]. This technology eliminates the need for surgery and associated post-implantation pain. In accordance with the authorized 433.1-434.8MHz, 902-928MHz, 2.4-2.5GHz, and 5.8GHz band frequencies assigned for industrial, scientific, and medical (ISM) bands, the operating frequency was selected [12]. In the present work, a fully integrated rectenna operating at 5.8GHz is introduced. The rectenna incorporates two different rectifier configurations designed with high-speed tunnel-based diodes. All rectenna components are monolithically integrated on a 600 µm-thick semi-insulating GaAs substrate. The

proposed topology achieves good performance in terms of DC output voltage and conversion efficiency compared with equivalent chip sizes reported in the literature. The present paper is organized as follows. In Section 2, the design and performance of the fabricated antenna are discussed in detail. Section 3 characterizes and analyzes the rectifier circuits. Section 4 presents the modeling results and discusses the fully integrated rectenna, along with a comparison with the literature. Section 5 presents the conclusion and summarizes the most important results achieved in the present work.

2.ANTENNA PERFORMANCE

The folded antenna was designed using the CST Studio electromagnetic tool to resonate at 5.8 GHz and then fabricated it using i-line photolithography. The simulation procedure was validated based on previous works demonstrated in [2, 10, 13]. Figure 1 depicts the 2D fabricated antenna geometry, showing the relevant dimensions designed and optimized for a miniaturized 1×5 mm² structure. The final dimensions of the antenna are tabulated in Table 1. The antenna sits on a high-permittivity (12.9) GaAs dielectric 600 µm thick. The red arrow in the middle of the structure represents the discrete feeding port used in the simulation routine. In a real-world rectenna circuit, the feeding port is replaced with a rectifier circuit, including an RC filter and probing pads for DC output measurements. Figure 2 depicts the antenna's 3D far-field radiation, with maximum gain and directivity of -14.6 dB and 2.54 dBi at the 5.8 GHz resonant frequency, respectively. These results indicate a low radiation efficiency (η_{rad}) of ~2.1%, mainly due to the very small effective radiating area of 5 mm². Unavoidable trade-offs exist between available antenna gain and small size, compounded by the L-shaped dipole formation. Nevertheless, the radiation efficiency (η_{rad}) data achieved exceeds 0.13% at 2.4 GHz with similar antenna dimensions as in [10], attributed to the higher operating frequency of 5.8 GHz. The antenna's overall performance is expected to improve significantly with a 2.5×10 mm² L-shaped structure, as discussed in [10]. In fact, a gain of around -15dB is reasonable for highly downscaled antenna geometries operating at ISM frequencies, as reported in medical implanted devices, with comparable gains reported [14-16]. According to Shahverdi et al. [17], a recent record for a triple-band antenna was -15dB, equivalent to the gain achieved here. For in-house test preparation, a calibration of the Vector Network Analyzer (Anritsu 37369A) was conducted before the measurement routine, eliminating systematic errors from RF cable losses and/or non-ideal probe impedance and establishing a reference plane at the probe tips for reliable, repeatable experimental data.

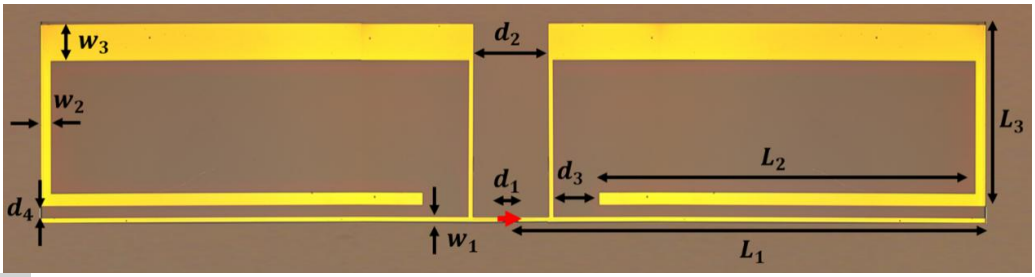


Fig. 1 2D Photomicrograph of the Fabricated 5.8 GHz Folded Antenna Structure, Indicating its Dimensions.

Table 1 Optimized Dimensions of the L-Shaped Antenna Designed in the Present Work.

Parameter	Value (µm)	Parameter	Value (µm)
L1	2400	W3	150
L2	1900	d1	100
L3	750	d2	500
W1	20	d3	230
W2	50	d4	50

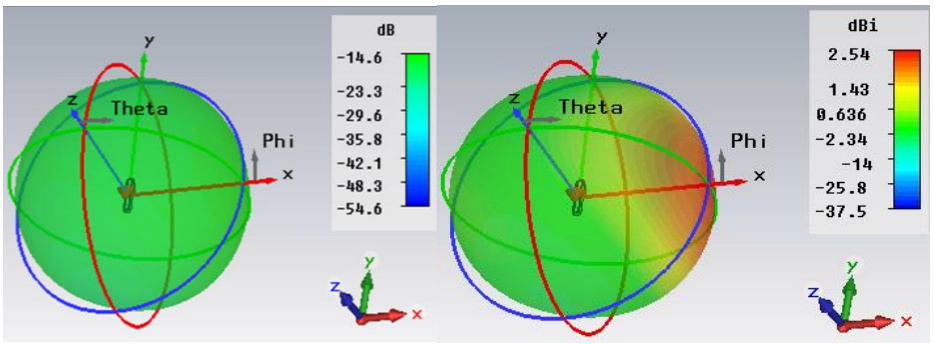


Fig. 2 3D far-Field Radiation of the 1×5 mm² Folded Antenna, with Simulated Gain (left-Hand Side) and Directivity (Right-Hand Side).

The measurement was performed using a GS (ground-signal) probe and open, short, and load dummy structures. Figure 3 reveals a good agreement between the measured and simulated results. The minimum measured return loss was -20 dB at 5.55 GHz, validating the present simulation model. The fabricated antenna shows a moderate bandwidth of nearly 480 MHz, spanning 5.38 to 5.86 GHz. Increasing the frequency bandwidth is vital to improving the rectenna circuit's energy-harvesting performance. A wide bandwidth provides benefits by capturing substantial power and maintaining a high data-rate transfer in wireless communication systems.

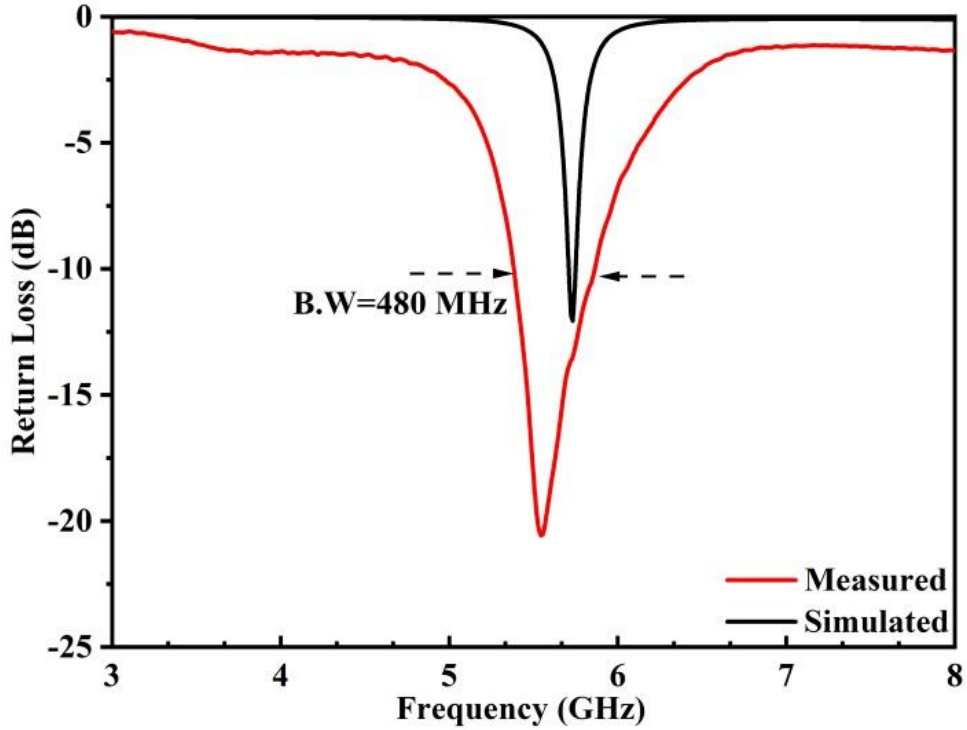


Fig. 3 Measured and Simulated Return Loss of the 1×5 mm² Folded Antenna Used in the Present Work.

3. VOLTAGE DOUBLER AND MULTIPLIER CHARACTERISATIONS

The integrated rectenna configuration comprises a folded antenna and a nonlinear diode to rectify the received RF signal and generate the DC output voltage required to supply the implantable devices. A simple rectifier circuit incorporates a single diode and an RC filter to bypass the higher order modes to ground, generated by the nonlinear behavior of the integrated diode. The filter also helps extract the DC voltage component at the output. However, a low output voltage is predicted from conventional rectifier networks due to further reduced antenna dimensions employed in biomedical fields. To overcome this challenge, a voltage doubler can be utilized, assisting to produce a doubled output voltage value benefited from the Cockcroft-Walton voltage doubler network. A similar topology has been explored in the 2.4 GHz ISM band frequency, with outstanding findings reported in [10]. The Cockcroft-Walton configuration uses two diodes to boost the amplitude of the received signal, as depicted in Fig. 4. The capacitors (C_1 and C_2) and the diodes (D_1 and D_2) represent a single stage of the voltage doubler. To further increase the amplitude voltage of the received signal, a proposed voltage multiplier based on the Dickson topology is investigated. The basic schematic of the Dickson circuit modeled in the present work is shown in Fig. 5.

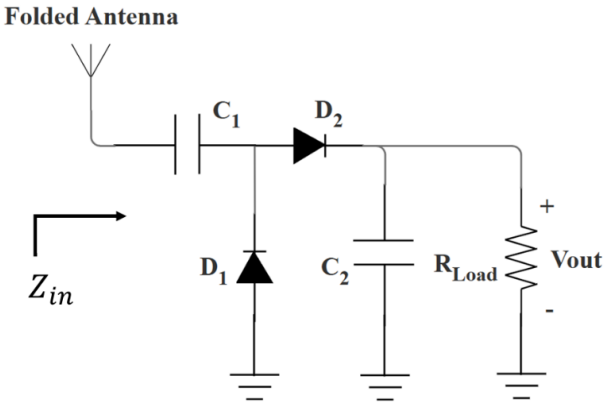


Fig. 4 Rectenna configuration with a single-stage Cockcroft-Walton doubler circuit.

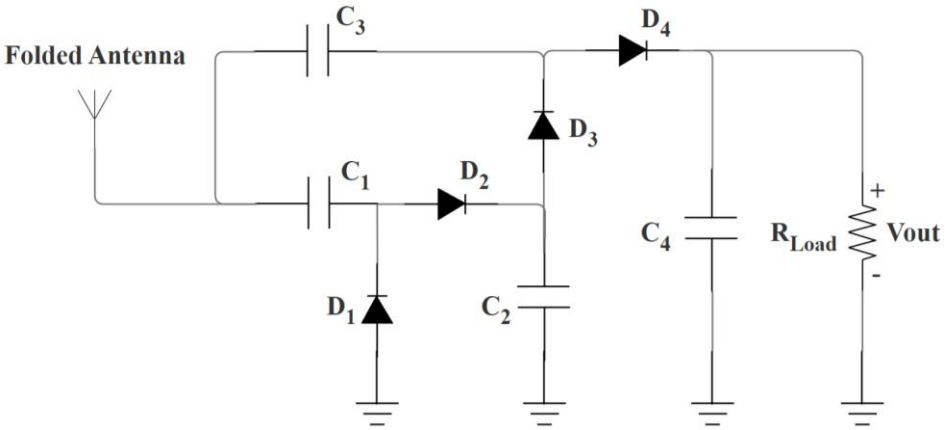


Fig. 5 Full Rectenna Schematic with a Two-Stage Dickson Multiplier Topology.

The doubler operation is summarized as follows. When an input sine-wave signal $V_{in} = V_{max}\, sin(\omega t)$, i.e., an amplitude of V_{max} is applied to the terminal, the negative half-cycle of the signal leads to forward-biases D_1, allowing to charge C1 capacitor via the D_1 with a $V_{max} - V_{D1}$, i.e., V_{D1} is the drop voltage across the diode. During the positive half-cycle, D_1 is reverse-biased and acts as an open circuit; meanwhile, D_2 is forward-biased, transferring the previously stored charge, $V_{max} - V_{D1}$, on C_1, along with the incoming $V_{max} - V_{D2}$ voltage, to the output capacitor C_2 via D_2. Therefore, the maximum output voltage can be doubled up to $2V_{max} - V_{D1} - V_{D2}$. For proper doubler operation, it is evidently imperative to reduce the voltage drop across the diodes. In the Dickson voltage multiplier, as shown in Fig. 5, a two-doubler-stage configuration boosts the output voltage to reach $4V_{max} - 4V_D$, assuming diodes D_1 to D_4 have the same voltage drop V_D.

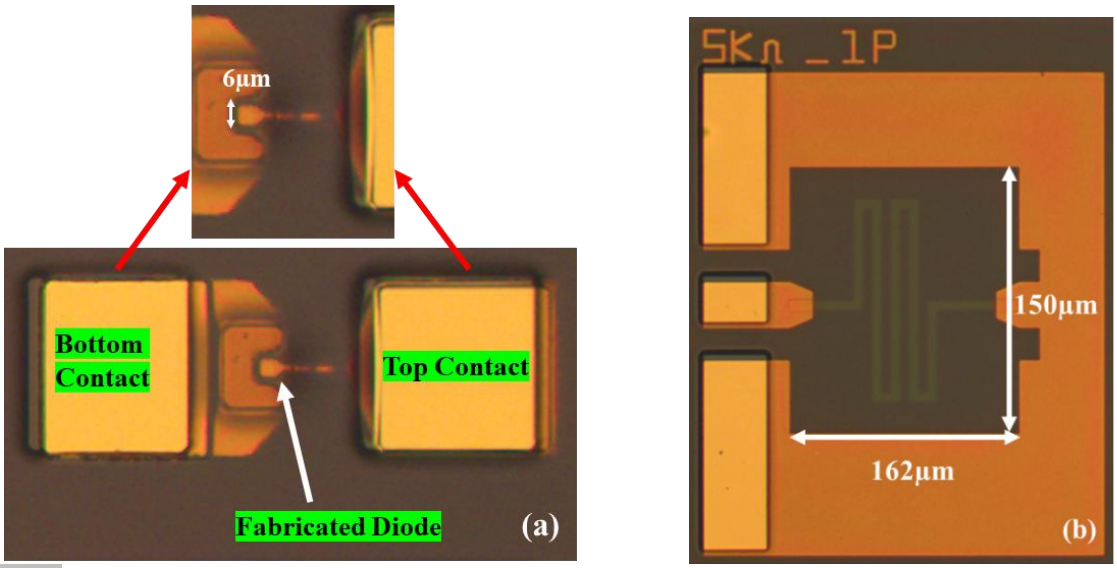


Fig. 6 Photomicrograph of the Fabricated Components: (a) A 36 µm² Diode with Top and Bottom Contacts Used for DC Measurement Probing, (b) a One-Port 5 kΩ Nichrome Resistor Designed Using a Meandering Structure.

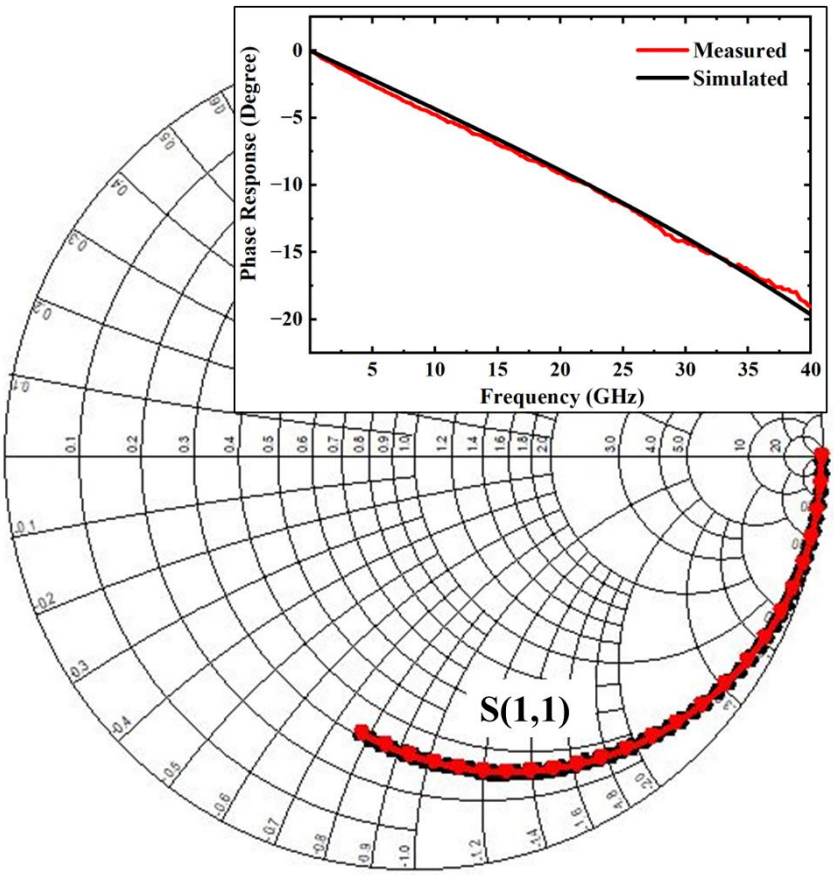


Fig. 7 Comparison Between the Simulated Equivalent-Circuit Model and Measured Reflection-Coefficient Results of a 36 μm² Tunnel Diode. Inset: Measured and Simulated Phase Response of a 5 kΩ Nichrome Resistor. The red and black Lines Represent Experimental and Simulated Data, Respectively.

Before simulating the rectenna model, the associated passive elements and integrated diodes were individually fabricated and tested. The results were used to develop an accurate model. A tunnel diode sample, XMBE#422, had a potential barrier of ~4 monolayers thick. A standard i-line photolithography technique and wet etching process were employed to fabricate all the components in a Class 1000 clean room. Several diode mesa sizes placed in a photomask design were successfully fabricated and measured, followed by the extraction procedure of the equivalent circuit model. Figure 6 (a) shows a fabricated diode device with a mesa size of 36 μm². The high-frequency measurement was conducted employing an on-wafer ground-signal-ground (GSG) probing technique up to 40 GHz. The equivalent-circuit model fits the measured data closely, as shown in Fig. 7; a similar approach is detailed in [18, 19]. The extracted series resistance (R_s) and junction capacitance (C_j) of the tunnel devices are tabulated in Table 2. Importantly, the data for the ≤16 μm² diodes were extrapolated from the experimental results of the large devices. The maximum operating frequency of the diodes can be estimated using $F_{cut-off} = 1/(2\pi R_s C_j)$. The 225 μm² devices had a 5 Ω series resistance and a 608 fF junction capacitance, resulting in an $F_{cut-off}$ of 52 GHz, and is extended to 126 and 250 GHz by downscaling the device dimensions to 36 and 9 μm², respectively. A micrometer-scale diode geometry could switch fast enough to meet the standard performance requirements of 5G frequency range 2 (FR2, allocated from 24.25 to 52.6 GHz) and/or mm-wave regime applications.

Table 2 Extracted equivalent circuit parameters from the measured data and evaluated cut-off frequency of the tunnel diode at zero-bias voltage used in the present work.

Device Mesa Size (μm²)	R_j (kΩ)	R_s (Ω)	C_j (fF)	$F_{cut-off}$ (GHz)
9	143	22	29	250
16	80	15	50	212
36	37	11	115	126
100	12.7	7.5	288	74
225	5.7	5	608	52

The performance and reliability of the passive elements were also paramount at high-frequency operation for the doubler and multiplier circuits because parasitic effects cause non-ideal responses; the fabrication process included a few passive elements, including 1 to 20 pF metal-insulator-metal capacitors and 1 to 20 kΩ nichrome resistors. An S-parameter testing routine was performed up to 40 GHz. Figure 6 (b) shows a 5 kΩ resistor designed with a meandering formation to reduce the resistor's overall length on the wafer

tile. The equivalent-circuit parameters of the resistors and capacitors were extracted and then included them in the full doubler/multiplier model. It can aid in preventing major design errors and improves simulation accuracy, bringing results in line with realistic measurements. The characterization steps of the passive elements conducted throughout the work are similar to those reported in [20, 21]. A validation of the simulation procedure has been fulfilled by the remarkable agreement between the experimental and model data, as shown in Fig. 7. To explore the fully integrated rectenna performance, the input impedance of the doubler circuit (Z_{in}) is required, initially determined from the configuration shown in Fig. 4. Accordingly, Z_{in} can be derived as expressed by:

$$\boldsymbol{Z_{in}} = \frac{R_s}{2} + \frac{R_j}{2+2\omega^2 C_j^2 R_j^2} - j\left(\frac{1}{\omega C_1} + \frac{\omega C_j R_j^2}{2+2\omega^2 C_j^2 R_j^2}\right) \quad \textbf{(1)}$$

Where ω is the angular frequency in rad/sec, given by ω=2πf, and f is the frequency. R_j is the junction resistance of the tunnel diode at zero-voltage bias, derived from the measured I-V curve ($R_j = dV/dI$). The impact of the RC filter given by the term $(1/j\omega C_2) \parallel R_{Load}$ was neglected and not included in Eq. (1) as the C_2 capacitor acts as a short circuit at the desired frequency. Corresponding to Eq. (1) and with the use of the extracted parameters in Table 2, the real and imaginary parts of Z_{in} were computed at 5.8GHz as a function of device size, as shown in Fig. 8. According to the results, the real part of the input impedance distinctly increased with the device size, as opposed to the imaginary component. The reactive component of Z_{in} exhibited a capacitive response; for instance, a 14-j481 Ω was achieved for a 9 μm² device, while revealing a 5-j55 Ω for a 100 μm² device, which is fundamental to determine before integrated antenna design, as impedance matching between the rectifier and antenna is crucial to minimize the amount of RF power being reflected to the transmitter. For a small device size of 9 μm², the impact of the operating frequency on Z_{in} is also valuable to evaluate to fully clarify the doubler's behavior. The dependency of both resistive and reactive components on frequency is evident, as depicted in Fig. 9. As expected, the real part increased as frequency decreased due to the ω^2 term in the denominator of the term $(R_s/2 + R_j/2\omega^2 C_j^2 R_j^2)$ at the given R_j and C_j values.

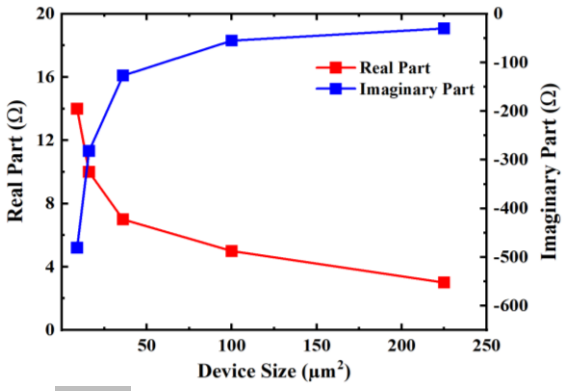


Fig. 8 Real and Imaginary Parts of the Evaluated Input Impedance of a Single Stage of Cockcroft-Walton Voltage Doubler as a Function of Tunnel Diode's Size.

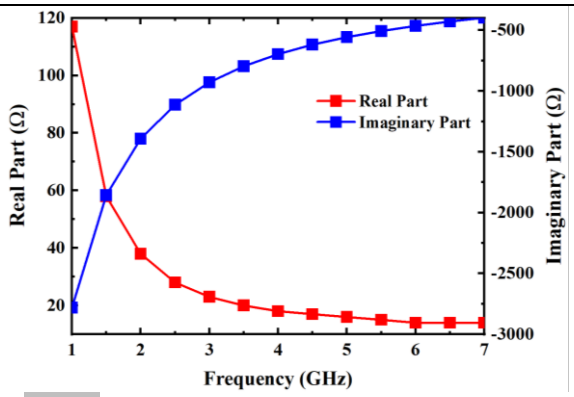


Fig. 9 Real and Imaginary Parts of the Input Impedance of a Single Stage of Cockcroft-Walton Voltage Doubler Designed with a 9 μm² Tunnel Diode as a Function of Frequency.

4.RECTENNA DESIGN AND RESULTS

With the extracted cut-off frequencies, the tunnel diode characterized in Section 3 is well suited to the band of interest for industrial, scientific, and medical applications. Incorporating a matching network with the antenna is key to maximizing the power delivered to the load. However, this design requires no matching circuit since the antenna arms were adjusted to ensure that the real part of the integrated rectifier and the antenna impedance are matched while still fulfilling the condition $|jX_{Ant} - jX_{input\ impedance}) = 0|$. As such, the primary inductive behavior of the antenna, jX_{Ant}, is compensated by the capacitive response of the doubler circuit, i.e., a negative reactance value, $-jX_{input\ impedance}$, as further discussed in [13], which not only simplifies the design steps by eliminating the need for matching stubs but also allows further reduction in the ultimate rectenna size. The measured data for the tunnel diode and the 1×5 mm² folded antenna were modeled in ADS (Advanced Design System) software to explore the doubler output voltage, as illustrated in the 2D circuit representation in Fig. 10. For the rectifier circuits, the passive elements were optimized to increase the DC output voltage at the load, as tabulated in Table 3. The optimization process in ADS software yielded a load resistor of 0.5 MΩ and a capacitor of 20 pF.

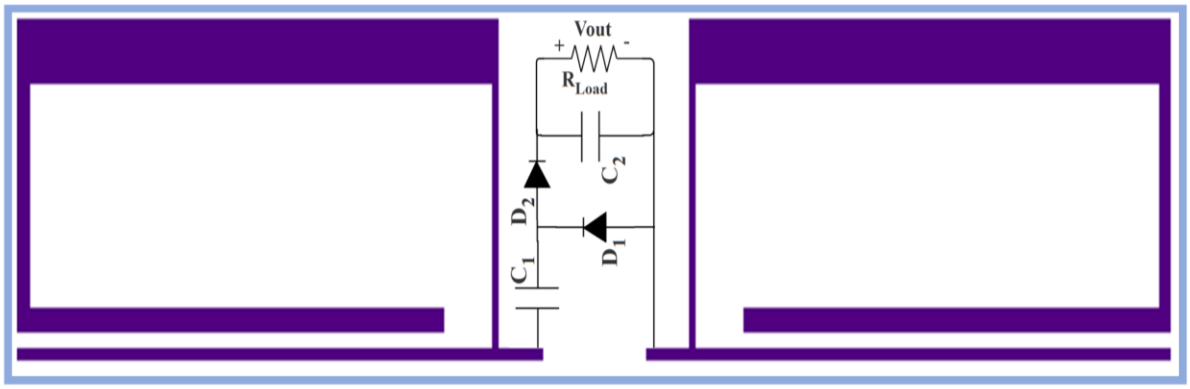


Fig. 10 Full rectenna structure with a single Cockcroft-Walton doubler configuration modeled in the present work.

Table 3 Extracted equivalent circuit parameters and evaluated cut-off frequency of the tunnel diode at zero-bias voltage used in the present work.

Rectifier type	C_1 (pF)	C_2 (pF)	C_3 (pF)	C_3 (pF)	R_{Load} (MΩ)
Cockcroft-Walton doubler	5	20	N/A	N/A	0.5
Dickson multiplier	10	10	10	20	0.5

Considering the rectifier result, antenna return loss, and the reflection response between them, RF-to-DC conversion efficiency is another crucial determinant of the rectenna's overall performance. It is obtained from the DC output power over the received RF power, as expressed by:

$$\eta_{RF-to-DC} = \frac{V_{DC}^2}{P_{RF} R_{Load}} \quad (2)$$

The conversion efficiency can be resulted from the DC output power over the received RF power. Figure 11 shows the DC output voltage of the rectenna simulated with a single-stage Cockcroft-Walton doubler. The load voltage (V_{DC}) increased with the applied RF power (P_{RF}), reaching a maximum value of 0.7 and 0.83 V at 0 dBm power for 36 and 9 μm² tunnel devices, respectively. These correspond to a reasonable RF-to-DC conversion efficiency of 0.098% and ~0.14%. A rectifier with a small tunnel device size showed a higher output voltage than circuits based on large diodes of ≥ 100 μm². These results are attributed to the impedance matching performance of the small-scale circuits, which is close to the standard 50 Ω antenna characteristic impedance, as shown in Fig. 8. It is found that the connected load resistor value significantly impacts the overall rectenna performance.

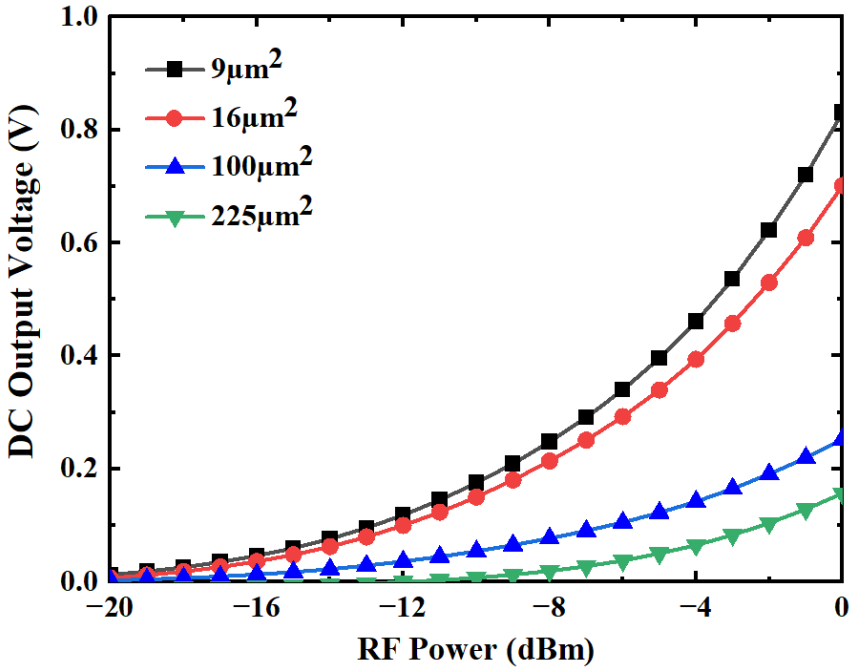


Fig. 11 Simulated DC Output Voltage of the 5.8 GHz Rectenna-Doubler with Different Integrated Device Sizes.

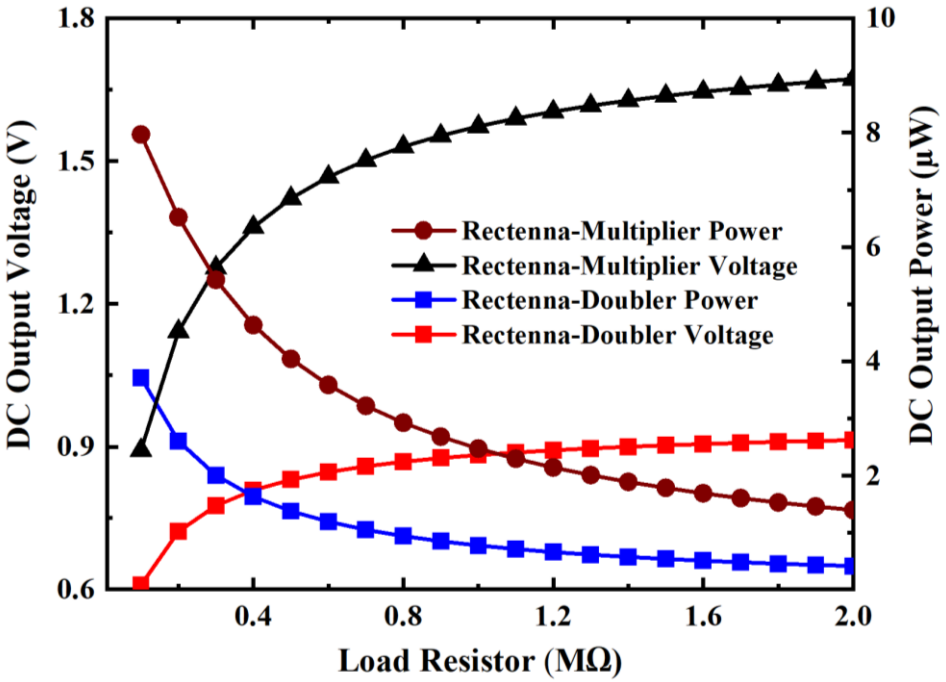


Fig. 12 Output Voltage and Power of the Voltage Rectenna-Doubler and Rectenna-Multiplier Built with 9 μm² Device Size. The Circuits Were Simulated at 0 dBm RF Power.

Figure 12 illustrates the rectenna's DC output power and voltage under different load resistors. A maximum power of 3.7 μW at 0 dBm received RF power was achieved with a 0.1 MΩ load, at the expense of a slight decrease in voltage to 0.61 V. Due to the opposite trend of the resulting power and voltage as a function of the connected load, a careful balance for the load resistor value is required, and that is mostly tailored to the application. To achieve high load power and improve RF-to-DC conversion efficiency in wireless power transfer systems, a voltage-multiplier-based Dickson rectifier topology was used. A similar simulation procedure performed with the doubler circuit was utilized in the extended rectifier configuration, with additional components in the Dickson multiplier; integration into a 1×5 mm² final chip size remained feasible, as the L-shaped antenna geometry with a 0.5 mm conductor spacing between the folded arms provides sufficient area for high-yield processing. A substantial increase in both output voltage and DC power simulated at 0 dBm RF power was achieved from the rectenna-multiplier circuit, as shown in Fig. 12. The variation in the load resistor implies that the optimum voltage and power of 1.25 V and 5.5 μW at ~0.25 MΩ were attainable, respectively, corresponding to an $\eta_{RF-to-DC}$ of 0.55 %, and can be extended to as high as 0.8 % at 0.1 MΩ load. A few antenna types, rectifier technologies, and integration schemes have been suggested in the literature towards achieving a miniaturized volume without significantly sacrificing implanted device performance.

Table 4 Performance of Compact Rectenna Technology Demonstrated in the Literature Operating in Industrial, Scientific, and Medical (ISM) Frequency Bands Compared with the Present Work.

Reported in	Antenna type/Rectifier technology	Frequency (GHz)	Chip size (mm²)	Power (Transmitted/Received)	RF-to-DC conversion efficiency (%)
[22]	Circular/Single Diode	1.47	9.6×9.6	1W/10.7mW	1.07
[23]	Circular/Doubler	2.45	10×10	1mW/1.39 μW	~0.139
[12]	Circular/Doubler	0.915	10.8×10.8	1W/4.3μW	0.00043
[24]	Spiral/Single Diode	0.402	20.5×31	0.5W/125μW	0.025
[25]	Coil/Multiplier	1.5	1.5×5	0.8W/0.83mW	0.1
[26]	Slotted patch/Doubler	1.9	5.6×6	1W/2.5mW	0.25
[9]	Spiral patch/Doubler	1.47	5×10	1W/6.7mW	0.67
[27]	Monopole/Multiplier with 5 stages	5.2	3.2×1.5	5W/100μW	0.002
[28]	Multiturn Dipole/Multiplier	5.8	3×1.5	4W/0.6μW	0.000015
This work	L-shaped Dipole/Doubler	5.8	1×5	1mW/1.38μW	~0.14
This work	L-shaped Dipole/Multiplier	5.8	1×5	1mW/8μW	0.8

An inclusive comparison between the proposed rectenna results and recently published papers is summarized in Table 4. Agrawal et al. [25] reported a chip size of 1.5×5 mm² and a low efficiency of 0.1% at a 1.5 GHz resonant frequency. A recorded $\eta_{RF-to-DC}$ of 0.67% was demonstrated at 1.47 GHz using a spiral patch antenna [9]; however, it used a full rectenna

area of 50 mm², ten times larger than the chip size proposed in the present work. At 5 GHz, the proposed design achieved a higher conversion efficiency of 0.8% than those reported in [27] and [28], with only 0.002% and 0.000015%, respectively, despite the use of five multiplier stages in [27].

5.CONCLUSIONS

A design and analysis of a 5.8 GHz L-shaped antenna integrated with doubler-multiplier configurations, targeting energy harvesting fields, has been presented. The focus was on miniaturizing the antenna dimensions achieved by incorporating a high-permittivity GaAs substrate and a long effective current path in the radiating patch. The effective design steps resulted in a very small antenna structure of only 5 mm², with 3D far-field radiation showing a maximum gain of -14.6 dB and directivity of 2.54 dBi at the resonant frequency. The low radiation efficiency of ~2.1% is due to the small antenna radiating size; however, it is still higher than that reported in a few works in the literature. The procedure followed here eliminates bulky matching networks, greatly easing circuit design and substantially reducing chip size. Simulation results for the rectenna-based voltage doubler showed a maximum DC output voltage and power of 0.61 V and 3.7 µW, respectively, at 0 dBm RF power and a 0.1 MΩ load resistor. These figures were boosted through employing the multiplier topology, delivering a maximum DC power of ~8 µW with an overall system efficiency of 8%. The proposed rectenna combines strong performance with a simple structure to design and fabricate, making it a strong candidate for low-power energy-harvesting systems, particularly for implanted medical devices. In the future, the goal is to integrate the rectenna with superstrate protective layers, enabling safe implantation of the final circuits inside the human body without causing medical risks.

CREDIT AUTHORSHIP CONTRIBUTION STATEMENT

Saad G. Muttlak: Writing – original draft, Visualization, Validation, Methodology, Formal analysis, Data curation, Conceptualization. ***Omar S. Abdulwahid***: Writing – review & editing, Methodology, Investigation. ***Mohammadreza Sadeghi***: Data curation. ***Mohamed Missous***: Supervision, Resources, Project administration, Funding acquisition.

DECLARATION OF COMPETING INTERESTS

The authors declare that they have no known competing financial interests or personal relationships that could have appeared to influence the work reported in this paper.

ACKNOWLEDGEMENTS

This research was supported by the European Union's Horizon 2020 research and innovation programme under grant agreement No 857654–UWIPOM2. "Ultra-Efficient Wireless Powered Micro-robotic joint (UWIPOM2)" and by the EPSRC through EP/P006973/1 "Future Compound Semiconductor Manufacturing Hub".

REFERENCES

[1] Deng X, Yang P, Chen S, Ren W. **Design of a 2.4 & 5.8 GHz Efficient Circularly Polarized Rectenna for Wireless Power Transfer Applications**. *Electronics* 2023; **12**(12): 2645.

[2] Walsh C, Muttlak SG, Sadeghi M, Missous M. **Miniature Integrated 2.4 GHz Rectennas Using Novel Tunnel Diodes**. *Sensors* 2023; **23**(14): 6409.

[3] Alamri S, AlAmoudi A, Langley R. **Gain Enhancement of Implanted Antenna Using Lens and Parasitic Ring**. *Electronics Letters* 2016; **52**(10): 800-801.

[4] Zhu S, Almari S, AlAmoudi AO, Langley RJ. **Implanted Antenna Efficiency Improvement**. *7th European Conference on Antennas and Propagation (EuCAP)* 2013; 3247-3248.

[5] Jasim M, Al-Gburi AJA, Hanif M, Dayo ZA, Ismail MM, Zakaria Z. **An Extensive Review on Implantable Antennas for Biomedical Applications: Health Considerations, Geometries, Fabrication Techniques, and Challenges**. *Alexandria Engineering Journal* 2025; **112**: 110-139.

[6] Lamkaddem A, El Yousfi A, González-Posadas V, Segovia-Vargas D. **Miniaturized Dual Band Implantable Antenna for Implanted Biomedical Devices**. *IEEE Access* 2024; **12**: 15026-15036.

[7] Hout S, Chung JY. **Design and Characterization of a Miniaturized Implantable Antenna in a Seven-Layer Brain Phantom**. *IEEE Access* 2019; **7**: 162062-162069.

[8] Wang Q, Chu H, Dang Y, Qiu J, Qi J. **A Compact 5.8 GHz Rectenna With High Conversion Efficiency Enabled by the Harmonic Suppression for Wireless Power Transfer**. *International Conference on Microwave and Millimeter Wave Technology (ICMMT)* 2022; 1-3.

[9] Basir A, Yoo H. **Efficient Wireless Power Transfer System with a Miniaturized Quad-Band Implantable Antenna for Deep-Body Multitasking Implants**. *IEEE Transactions on Microwave Theory and Techniques* 2020; **68**(5): 1943-1953.

[10] Muttlak SG, Sadeghi M, Ian K, Missous M. **Low-Cost Compact Integrated Rectenna for Implantable Medical**

Receivers. *IEEE Sensors Journal* 2022; **22**(17): 16938-16944.

[11] Troyk PR. **Injectable Electronic Identification, Monitoring, and Stimulation Systems**. *Annual Review of Biomedical Engineering* 1999; **1**(1): 177-209.

[12] Ding S, Koulouridis S, Pichon L. **Miniaturized Implantable Power Transmission System for Biomedical Wireless Applications**. *Wireless Power Transfer* 2020; **7**(1): 1-9.

[13] Muttlak SG, Sadeghi M, Ian K, Missous M. **Miniaturized Folded Antenna with Improved Matching Characteristic for Mm-Wave Detections**. *14th UK-Europe-China Workshop on Millimetre-Waves and Terahertz Technologies (UCMMT)* 2021; 1-3.

[14] Feng Y, Li Z, Qi L, Shen W, Li G. **A Compact and Miniaturized Implantable Antenna for ISM Band in Wireless Cardiac Pacemaker System**. *Scientific Reports* 2022; **12**(1): 238.

[15] Iqbal A, Al-Hasan M, Mabrouk IB, Nedil M. **A Compact Implantable MIMO Antenna for High-Data-Rate Biotelemetry Applications**. *IEEE Transactions on Antennas and Propagation* 2021; **70**(1): 631-640.

[16] Fan Y, Liu X, Xu C. **A Broad Dual-Band Implantable Antenna for RF Energy Harvesting and Data Transmitting**. *Micromachines* 2022; **13**(4): 563.

[17] Shahverdi K, Hashemi S, Sarafan S, Cao H. **Triple-Band Implantable Antenna Design for Biotelemetry Applications in MICS/ISM/Wi-Fi/Bluetooth Bands**. *Technologies* 2022; **10**(4): 91.

[18] Cho H, Burk DE. **A Three-Step Method for the De-Embedding of High-Frequency S-Parameter Measurements**. *IEEE Transactions on Electron Devices* 1991; **38**(6): 1371-1375.

[19] Chen Q, Chen X, Cai H, Chen F. **Schottky Diode Large-Signal Equivalent-Circuit Parameters Extraction for High-Efficiency Microwave Rectifying Circuit Design**. *IEEE Transactions on Circuits and Systems II: Express Briefs* 2020; **67**(11): 2722-2726.

[20] Sharma R, Vinayak S, Rawal D, Kumar A, Ray U. **RF Parameter Extraction of MMIC Nichrome Resistors**. *Microwave and Optical Technology Letters* 2003; **39**(5): 409-412.

[21] Wang L, Xu RM, Yan B. **MIM Capacitor Simple Scalable Model Determination for MMIC Application on GaAs**. *Progress in Electromagnetics Research* 2006; **66**: 173-178.

[22] Iqbal A, Al-Hasan M, Mabrouk IB, Basir A, Nedil M, Yoo H. **Biotelemetry and Wireless Powering of Biomedical Implants Using a Rectifier Integrated Self-Diplexing Implantable Antenna**. *IEEE Transactions on Microwave Theory and Techniques* 2021; **69**(7): 3438-3451.

[23] Sharma D, Kumar S, Singh N, Kanaujia BK. **Far-Field Wireless Power Transmission and Measurement for a Leadless Transcatheter Pacing System**. *IEEE Transactions on Instrumentation and Measurement* 2023; **72**: 1-12.

[24] Das R, Yoo H. **A Multiband Antenna Associating Wireless Monitoring and Nonleaky Wireless Power Transfer System for Biomedical Implants**. *IEEE Transactions on Microwave Theory and Techniques* 2017; **65**(7): 2485-2495.

[25] Agrawal DR, Tanabe Y, Weng D, Ma A, Hsu S, Liao SY, Zhen Z, Zhu ZY, Sun C, Dong Z, Yang F, Tse HF, Poon ASY, Ho JS. **Conformal Phased Surfaces for Wireless Powering of Bioelectronic Microdevices**. *Nature Biomedical Engineering* 2017; **1**(3): 0043.

[26] Shah SAA, Yoo H. **Radiative Near-Field Wireless Power Transfer to Scalp-Implantable Biotelemetric Device**. *IEEE Transactions on Microwave Theory and Techniques* 2020; **68**(7): 2944-2953.

[27] Ouda MH, Arsalan M, Marnat L, Shamim A, Salama KN. **5.2 GHz RF Power Harvester in 0.18-μm CMOS for Implantable Intraocular Pressure Monitoring**. *IEEE Transactions on Microwave Theory and Techniques* 2013; **61**(5): 2177-2184.

[28] Radiom S, Baghaei-Nejad M, Aghdam KM, Vandenbosch GAE, Zheng LR, Gielen GGE. **Far-Field On-Chip Antennas Monolithically Integrated in a Wireless-Powered 5.8 GHz Downlink/UWB Uplink RFID Tag in 0.18-μm Standard CMOS**. *IEEE Journal of Solid-State Circuits* 2010; **45**(9): 1746-1758.